JOURNAL OF CATALYSIS 148, 240–251 (1994)

Potential-Programmed Reduction: A New Technique for Investigating the Thermodynamics and Kinetics of Chemisorption on Catalysts Supported on Solid Electrolytes

Yi Jiang,[1] Ioannis V. Yentekakis, and Constantinos G. Vayenas[2]

Institute of Chemical Engineering and High Temperature Chemical Processes, Department of Chemical Engineering, University of Patras, Patras GR-26500, Greece

Received December 2, 1993; revised February 18, 1994

A new technique is presented for investigating the kinetics and thermodynamics of chemisorption of oxygen and, potentially, of other adsorbates on conductive catalyst films deposited on solid electrolytes, such as yttria-stabilized zirconia, an O^{2-}conductor. In this technique, termed potential-programmed reduction (PPR), the catalyst surface is first exposed to the chemisorbing gas and then the catalyst potential is swept linearly by, typically -1 V, causing the reduction of chemisorbed oxygen to O^{2-} at distinct and well-resolved catalyst potential values E_p. In this way current peaks centered at E_p are generated. The area of each peak provides direct quantitative information about the coverage of adsorbed oxygen and the corresponding E_p value about its Gibbs free energy. The PPR technique has certain similarities with temperature-programmed reduction but is isothermal and provides direct thermodynamic as well as kinetic information. It is, however, limited to conductive catalyst films which can be supported on solid electrolytes. In the present work the PPR technique is used to investigate oxygen chemisorption on Ag and Pt. In the case of Ag two types of oxygen are resolved at temperatures 300 to 450°C (atomically adsorbed and subsurface), while on Pt there is usually one peak corresponding to atomic oxygen with a second peak developing after prolonged exposure to positive potentials.

INTRODUCTION

Solid electrolyte cells have been used extensively in catalytic research during the last fifteen years. Work in this area has been reviewed recently (1). Their first application to measure *in situ* the thermodynamic activity of oxygen on metal catalysts was originally proposed by Wagner (2). This led to the technique of solid electrolyte potentiometry (SEP) which has been used in conjunction with kinetic measurements to study a number of catalytic reactions on metals (3–8) and is particularly useful for the study of oscillatory reactions (5, 8, 9). Recent experimental (10, 11) and theoretical work (1) has shown that solid electrolyte cells can be used both as work function probes and as work function controllers for their gas-exposed metal electrode surfaces (1, 10, 11). It should be noted that similar types of solid electrolyte cells with appropriately chosen electrodes can be operated in the fuel cell mode for power generation (12, 13) or for chemical cogeneration (14–16), i.e., for the simultaneous production of electrical power and chemicals, e.g., NH_3 oxidation to NO (14) or H_2S oxidation to SO_2 (16), as also reviewed recently (1).

From a catalytic viewpoint the most interesting application of solid electrolyte cells is their active or oxygen pump mode of operation, i.e., external voltage or current application to cells of the type

gaseous reactants, metal catalyst/ZrO_2

$$(8\ \text{mol}\%Y_2O_3)/M, O_2$$

to affect the catalytic activity of the catalyst. It has been found that the activity and selectivity of metal catalysts can be altered dramatically and in a reversible manner by electrochemically pumping oxygen anions to or from catalyst surfaces (1, 11, 17–29). The increase in catalytic rate can be up to 100 times larger than the regular (open-circuit) catalytic rate and up to 3×10^5 times larger than the rate of ion supply to the catalyst (1, 11, 17–29). The effect has been termed non-Faradaic electrochemical modification of catalytic activity (NEMCA effect), electrochemical promotion in catalysis (30), or *in situ* controlled promotion (27). Work in this area has been reviewed recently (1).

Recent application of cyclic voltammetry in solid electrolyte cells (31–35) has shown that the technique can be used both for studying the NEMCA effect (31) and for investigating different oxidation states of metals (33–35).

In the present communication we report that the use of the same type of solid electrolyte cells in conjunction

[1] On leave from Dalian Institute of Chemical Physics, CAS, Dalian, China.

[2] To whom correspondence should be addressed.

0021-9517/94 $6.00

with the linear potential sweep technique (36) provides the means to examine *in situ* different oxygen species chemisorbed on metal catalysts and to study both their thermodynamics and their desorption kinetics. Cyclic voltammetry as well as the similar linear potential sweep technique (36) are powerful techniques used routinely in aqueous electrochemistry to study redox reactions on electrodes. Because of the aqueous electrolyte involved, previous applications of the linear potential sweep technique have been limited to low temperatures where only electrocatalytic (net charge-transfer) and not catalytic reactions take place on the electrodes. The use of solid electrolytes makes it possible to use electrochemical reactions at temperature of catalytic interest and thus to study the chemisorptive and catalytic phenomena taking place on the gas-exposed catalyst-electrode surfaces. Therefore, electrochemical techniques, such as linear potential sweep, can be applied to study heterogeneous reactions at high temperatures (250–750°C).

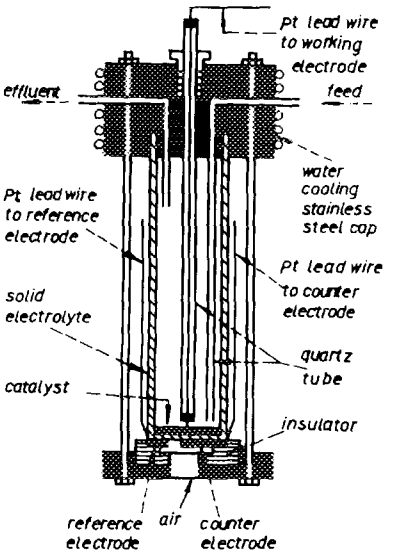

FIG. 2. Zirconia adsorption cell.

EXPERIMENTAL

Catalyst and Apparatus

The experimental apparatus is shown schematically in Fig. 1. The central part of the apparatus is the 8 mol% yttria stabilized zirconia (YSZ) tube continuous flow reactor (adsorption cell) shown in Fig. 2. Within the experimental space time range used in the present study the reactor, with volume of 30.3 cm^3, has been shown to behave as a continuously stirred tank reactor (CSTR) as described in previous papers (5, 8, 17). A potentiostat–galvanostat (AMEL 553) in conjunction with a function generator (AMEL 567) was used to generate linear variation in time of the potential of the working electrode with respect to the reference electrode. The oxygen content of effluent gas was analyzed via on-line gas chromatography (Perkin–Elmer Sigma 3000) and mass spectrometry (Balzers QMG 311). At temperatures below 1200°C YSZ is a pure O^{2-} conductor (1).

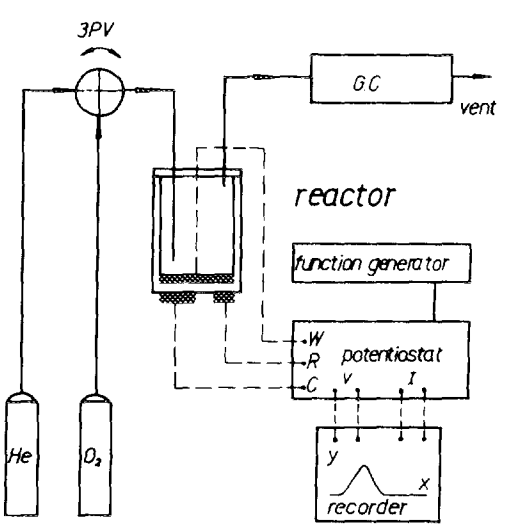

FIG. 1. Schematic diagram of the apparatus.

The catalyst film under study is deposited on the inside bottom wall of the stabilized zirconia tube and acts as the working electrode. Reference and counter electrodes are prepared on the outside bottom wall of the tube using either the same material with the working electrode or other suitable electrocatalytic materials (1). In this form of three-electrode system, the working electrode(catalyst) is exposed to the chemisorbing gas, in the present case O_2, while the counter and reference electrodes are exposed to ambient air, so that the potential of the reference electrode remains constant during the experiments.

Catalysts investigated in this paper were platinum and silver. It is also possible to deposit other catalysts such as metal oxides on the solid electrolyte as reported in other studies (33–35). Details of Pt catalyst film preparation have been described previously (8). The procedure is to use a thin coating of Englehard A1121 Pt paste followed by drying and calcining in air for 2 h at 400°C and then for 30 min at 820°C. The Ag catalyst film was prepared by depositing a thin coating of Ag solution in butyl acetate (GC electronics 201) followed by drying at 80°C and calcining at 600°C for 2 h (1, 20–22). Reference and counter electrodes were prepared from the same material as the working electrode in exactly the same way. Previous XPS experiments have shown no detectable metal impurities in catalyst films prepared by this procedure (4, 8, 17, 28).

Experimental Procedure

The experiments were conducted isothermally at temperatures 340–500°C. The isothermal experimental procedure consisted of the following steps:

I. Application of a negative potential (−800 mV with respect to the O_2 (21 kPa), M (Pt or Ag)/YSZ reference electrode) under ultrapure He (99.999%) flow in order to remove any residual oxygen from the catalyst film surface.

II. Catalyst exposure to a 21% O_2–79% He mixture at a space time of 36 s for oxygen adsorption. The time of exposure, hereafter denoted by t_{O_2}, was typically on the order of 100–1000 s. During this step, as well as during the next step, the catalyst was maintained under open circuit conditions.

III. Catalyst exposure to ultrapure He for a time period, hereafter denoted by t_{He}, typically of the order 100–500s. During this step the gas phase of the cell is cleaned from gaseous oxygen. This is why t_{He} was chosen to be typically 5 to 10 times longer than the gas residence time in the cell (cell volume 30.3 cm^3, He flowrate 2 cm^3 STP/s) as in previous isothermal titration studies (1, 21). The gas phase is essentially oxygen-free after the first three residence times. During t_{He} oxygen desorption from the catalyst is taking place and, in fact, as shown below the kinetics of oxygen desorption can be studied by varying t_{He}.

IV. Linear potential sweep application starting from the open-circuit potential $V_{WR} = V^0_{WR}$ (typically −30 to −200 mV) and reaching $V_{WR} = -1$ V. The potential V_{WR} is swept linearly at a sweep rate v, typically 3–100 mV/s, i.e.,

$$V_{WR} = V^0_{WR} - v \cdot t. \qquad [1]$$

During this step oxygen species adsorbed on the metal at or near the three-phase-boundaries (tpb) metal catalyst—YSZ–gas are reduced to O^{2-}, which migrate to the YSZ lattice

$$O(a) + 2e^- \rightarrow O^{2-}, \qquad [2a]$$

or, in Kröger–Vink notation (1), frequently used in the solid state literature,

$$O(a) + V_O^{\cdot\cdot} + 2e' \rightarrow O_O, \qquad [2b]$$

where $V_O^{\cdot\cdot}$ and O_O stand for lattice vacancy and lattice oxygen, respectively.

When the potential V_{WR}, which is swept linearly according to Eq. [1], reaches the vicinity of the equilibrium potential of an adsorbed oxygen species, then the charge transfer reaction (2) takes place until the adsorbed oxygen species is completely depleted and thus a (negative) current I is generated which, when recorded as a function of the varying V_{WR}, gives rise to well-resolved peaks, i.e., to the potential-programmed reduction (PPR) spectra.

During the present investigation we have also studied an alternative way of supplying oxygen to the catalyst surface, instead of step (II); i.e., a positive current or potential was applied to the cell under He catalyst exposure conditions and thus adsorbed oxygen O(a) was generated via the reverse of reaction (2), i.e.,

$$O^{2-} \rightarrow O(a) + 2e^-. \qquad [3]$$

It should be noted that the PPR technique bears several similarities with temperature-programmed desorption (TPD) and temperature-programmed reduction (TPR) which are commonly used in catalysis research. The main differences of PPR from the TPD and TPR techniques are the following.

I. In PPR it is the catalyst potential (and work function (1, 10, 11)) which is varied linearly in time instead of temperature.

II. In PPR the adsorbed oxygen species are reduced electrochemically to O^{2-} instead of desorbing or reacting catalytically with a reducing species.

The main advantage of PPR is that it is isothermal and can give direct kinetic and thermodynamic information about adsorbed species. The theory of linear potential sweep voltammetry is well developed in aqueous electrochemistry (26–38) and can be used for data interpretation in solid electrolyte systems as well (31, 32). The main disadvantage of PPR is that it is limited to conductive catalysts supported on solid electrolytes.

RESULTS AND DISCUSSION

Ag Catalyst Films

Typical PPR spectra of oxygen adsorbed on Ag are shown in Fig. 3. They were all obtained for $t_{O_2} = 300$ s and $v = 10$ mV/s starting from the open-circuit potential ($V_{WR} = V^0_{WR}$, $I = 0$) and terminating at $V_{WR} = -0.9$ V. Two well-resolved peaks, labeled A and B are obtained for short desorption (t_{He}) times. Peak A is centered at $E_p = -120$ mV and peak B at $E_p = -240$ mV. Longer oxygen desorption time t_{He} leads to a substantial decrease

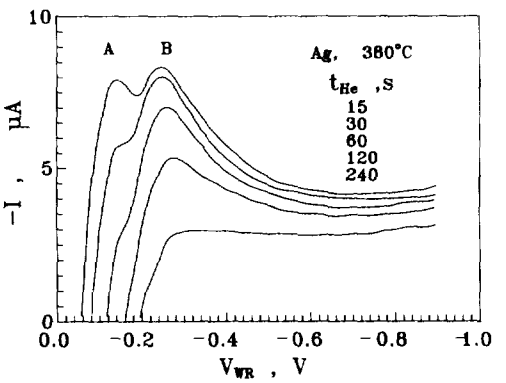

FIG. 3. Effect of desorption time t_{He} on the PPR spectrum of oxygen adsorbed on Ag after exposure to gaseous O_2; $v = 10$ mV/s, $F_{He} = 100$ cm^3 STP/min.

in the area of both peaks until at t_{He} = 240 s only a background current is obtained (Fig. 3). Peak A disappears faster than peak B.

It is also worth noting in Fig. 3 that the open-circuit catalyst potential (I = 0, $V_{WR} = V^0_{WR}$) shifts gradually to more negative values with increasing t_{He}. This is because V^0_{WR} is determined via the Nernst equation (1–6)

$$V^0_{WR} = \frac{RT}{2F} \ln [a_O/(0.21)^{1/2}] \quad [4]$$

by the activity a_O of oxygen adsorbed on the Ag catalyst, where F is Faraday's constant and 0.21 is the activity of gaseous oxygen at the reference electrode. Consequently the decrease in V^0_{WR} with t_{He} is due to the desorption of oxygen from the catalyst and to the concomitant decrease in oxygen activity. It is worth noting in Fig. 3 and subsequent figures that a peak disappears with increasing t_{He} when V^0_{WR} drops below the characteristic peak maximum potential value, denoted by E_p. This is because each E_p value corresponds, provided the peak is "reversible" (31, 32, 36) as discussed below, to a certain, characteristic for each adsorbed oxygen species, oxygen activity (or oxygen chemical potential) value and thus when the surface oxygen activity is below this characteristic value the corresponding oxygen species cannot remain adsorbed on the surface.

Figure 4 shows PPR spectra of oxygen adsorbed on Ag obtained by "electrochemical oxygen dosing" of the catalyst surface via reaction (3), i.e., by applying a small (0.2 V) positive potential and thus supplying the adsorbing oxygen via the solid electrolyte instead of via the gas phase. As can be seen by comparing Figs. 3 and 4 both methods result in the same PPR spectra. This shows that "electrochemical dosing" can be used to simulate oxygen adsorption from the gas phase provided the applied overpotential is small (0.2 V) to avoid the complications arising from the generation of anionic oxygen spillover species causing NEMCA (28). Electrochemical oxygen dosing is more convenient for obtaining PPR spectra than gas phase dosing because in this way the entire experiment is carried out under continuous ultrapure He flow. Thus in subsequent PPR spectra, unless otherwise specified, oxygen was dosed through the electrolyte.

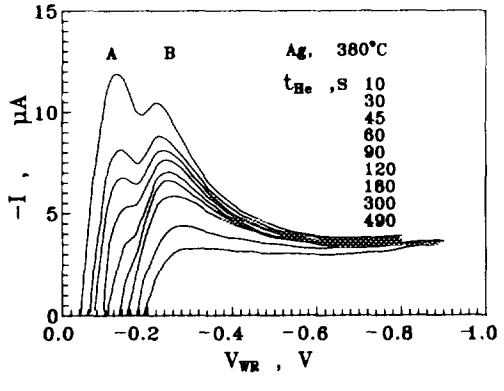

FIG. 4. Effect of desorption time t_{He} on the PPR spectrum of oxygen adsorbed on Ag after electrochemical supply of oxygen (V_{WR} = 0.2 V for 60 s); conditions as in Fig. 3.

The two oxygen peaks A and B in the PPR spectra of Figs. 3 and 4 show clearly the existence of two different oxygen species on the Ag catalyst. The significant (120 mV) difference in the peak potential E_p values shows substantially different thermodynamic properties for the two oxygen species; i.e., species A has significantly higher chemical potential and thermodynamic activity than species B and is also more active for desorption and for electrochemical reduction.

Previous studies of the adsorption of oxygen on Ag surfaces (21, 39–45) and in particular the use of TPD, isotope exchange and XPS have clearly established the existence of three main types of oxygen on Ag, i.e., molecular, atomic, and subsurface oxygen.

Molecular oxygen, usually termed α-state oxygen in TPD spectra (39), desorbs at temperatures below 200°C (39, 40) and therefore could not be observed in the present study, since ionic conductivity considerations limit the use of the present technique to temperatures above 300°C.

Atomic oxygen, i.e., β-state oxygen in TPD spectra (39), is the active species for most Ag-catalyzed partial and complete oxidation reactions (40, 44) and desorbs at temperatures around 350°C (40). It gives rise to peak A of the present investigation according to the reaction:

$$O(a) + V_O^{\cdot\cdot} + 2e' \rightarrow O_O. \quad [5]$$

Peak B is therefore due to the third type of oxygen on Ag, i.e., subsurface oxygen usually denoted as γ-state oxygen in TPD spectra (39). Subsurface oxygen is known to affect significantly the chemisorptive properties of Ag surfaces (40). Its presence is a necessary condition for obtaining high selectivity to ethylene oxide during ethylene epoxidation. It gives rise to a broad TPD peak centered near 600°C (39), rapidly exchanges with atomic oxygen (39), and can be slowly cleaned off by reaction with CO (40) or with C_2H_4 (21).

Effect of oxygen dosing time and potential sweep rate. Before discussing the kinetic and thermodynamic information which can be extracted from PPR spectra, it is useful to first describe the effect of two important operational variables on the quality of PPR spectra.

The first variable is the amount of oxygen dosed on the surface, which dictates the oxygen coverage at the tpb. As shown in Fig. 5 increasing oxygen coverage obtained by increasing the holding time t_H at a mildly positive potential has a very small effect on the peak potentials

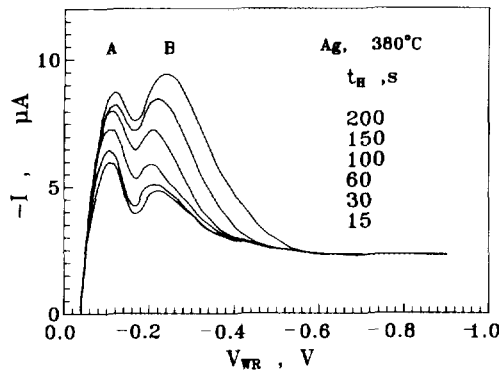

FIG. 5. Effect of potential holding time t_H at V_{WR} = 0.2 V on the PPR spectrum of oxygen adsorbed on Ag; t_{He} = 10s; v = 5 mV/s, F_{He} = 100 cm^3 STP/min.

E_p for the case of oxygen adsorption on Ag. This is not the case for Pt as discussed below. The insensitivity of E_p on the amount of oxygen dosed in the case of Ag suggests weak lateral adsorbate interactions. Consequently, increasing holding time t_H increases the height of the peaks but has very small effect on their position.

The second operational variable which seriously affects the quality of PPR spectra is the potential sweep rate v. An example is shown in Fig. 6. Decreasing sweep rate v improves significantly the separation of the two peaks A and B. This is because at the limit of very low v values the PPR peaks become reversible in the electrochemical sense (32, 36); i.e. the same E_p value is obtained in the anodic ($I > 0$) and cathodic ($I < 0$) potential sweep and then E_p is a true thermodynamic quantity. For high sweep rate values, E_p decreases due to electrokinetic considerations (32, 36) and conveys no useful thermodynamic information (36). All the E_p values reported below and denoted by $E_{p,rev}$ are extrapolated E_p values for v = 0. Thus, in general, as low v values as possible must be used in PPR. However decreasing v causes an increase in the desorption time and thus a decrease in the amount of adsorbed oxygen and in peak height (Fig. 6). Consequently, an optimal compromise must be sought in each system to ensure both high signal and reversibility, i.e., constant E_p.

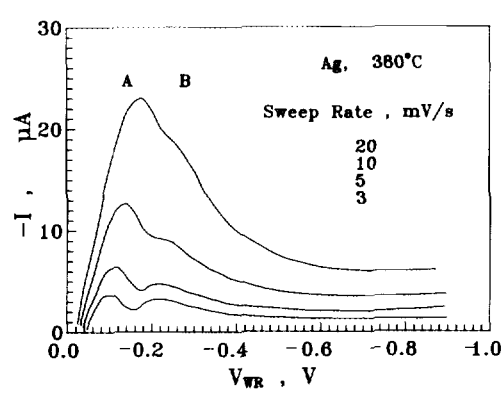

FIG. 6. Effect of sweep rate v on the PPR spectrum of oxygen adsorbed on Ag; t_H = 30 s, V_{WR} = 0.2 V, t_{He} = 10 s, F_{He} = 100 cm^3 STP/min.

Desorption Kinetics

As shown already in Figs. 3 and 4, increasing desorption time t_{He} causes a more pronounced decrease in peak A than in peak B. This is reasonable in view of the fact that chemisorbed atomic oxygen is expected to desorb faster than subsurface oxygen (21, 40).

The peak areas in PPR spectra, corrected for the residual current, provide a direct measure of the total charge associated with the reduction of adsorbed species at the vicinity of the tpb Ag–solid electrolyte–gas. This was verified by repeating the potential sweep and obtaining no residual oxygen peaks.

Consequently the amount of oxygen adsorbed at the vicinity of the tpb (atomic oxygen or subsurface oxygen) can be computed from

$$N_{O,tpb} = \frac{\int_A I dt}{2F} = \frac{\int_A I dE}{2vF} \quad [6a]$$

$$N_{O,sub,tpb} = \frac{\int_B I dE}{2vF}, \quad [6b]$$

where v is the sweep rate (mV/s). The usefulness of Eq. [6] for estimating the length l of the three-phase-boundaries metal–YSZ–gas has been discussed previously (31). For most metals (1, 21, 31) the parameter l is proportional to the exchange current I_0 of the metal–YSZ interface. This parameter is important both for NEMCA studies (1) and for the performance of solid oxide fuel cells (1, 12, 13).

Figure 7 depicts the kinetics of desorption of atomic oxygen and subsurface oxygen obtained from Figs. 3 and

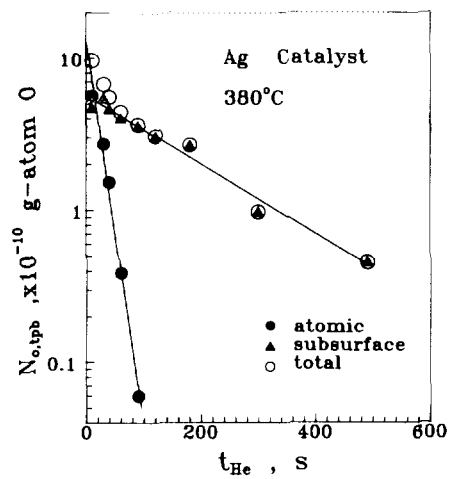

FIG. 7. Kinetics of desorption of atomic oxygen and subsurface oxygen.

4 via Eqs. [6]. Both types of oxygen exhibit near first-order desorption from the entire electrode surface by using the isothermal surface titration technique (1, 21). The first-, rather than second-, order desorption kinetics are due to the high oxygen coverages (1). The apparent first-order desorption rate constants k_d extracted from Fig. 7 for atomic and subsurface oxygen are 5.9×10^{-2} s^{-1} and 5.2×10^{-3} s^{-1}, resepctively, at 380°C.

Figure 8 shows the desorption kinetics of atomic oxygen at various temperatures. In all cases first order kinetics are observed. The intersect at $t_{He} = 0$ gives the maximum amount of atomic oxygen adsorbed at the tpb ($N_{O,tpb} \approx 10^{-9}$ g-atom O). For comparison purposes the total maximum amount of oxygen adsorbed on the entire gas-exposed Ag catalyst surface was measured via the isothermal surface titration technique and found to equal $N_O = 3 \times 10^{-7}$ g-atom O. Consequently the electrocatalytically active surface area of the Ag catalyst film (tpb plus adjacent sites) accounts for 0.3% of the total catalyst surface area in qualitative agreement with previous results and theoretical models (31).

Figure 9 shows the temperature dependence of the desorption rate constant of atomic oxygen. The activation energy for desorption extracted from the Arrhenius plot is 20 kcal/mol, which is lower than most literature values for the β-state (atomic oxygen) obtained via TPD under UHV conditions (39, 40, 45), i.e., 30–35 kcal/mol, but closer to values obtained via isothermal desorption and titration under atmospheric pressure conditions at high oxygen coverages (4, 6). In fact, as also shown in Fig. 9, the measured k_d values are in very good agreement with literature k_d values for atomic oxygen desorption from the entire Ag catalyst surface of similar YSZ-supported Ag films using the isothermal desorption titration technique (4, 6). This shows that no significant difference exists in the binding energy and thermodynamics of oxygen adsorbed at the tpb and over the entire gas-exposed catalyst surface.

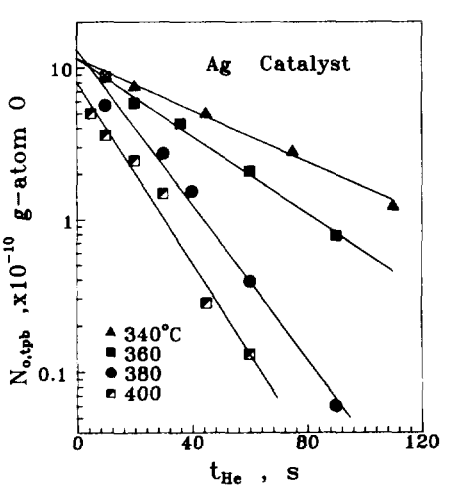

FIG. 8. Effect of temperature on the desorption kinetics of atomic oxygen.

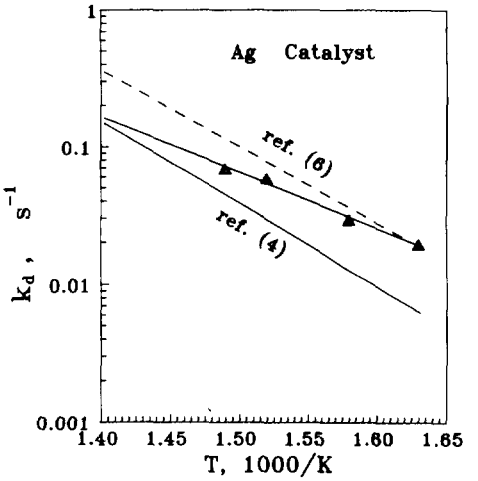

FIG. 9. Temperature dependence of the desorption rate constant of atomic oxygen k_d and comparison with literature values of k_d for desorption from the entire gas-exposed Ag electrode surface.

Thermodynamics of adsorption. The peak potentials E_p convey useful thermodynamic information, to the extent that the sweep rate v is slow enough so that the peak is reversible (36).

Under such conditions E_p is related to the chemical potential $\mu_{O_2(a)}$ of the adsorbed oxygen species being reduced via:

$$E_p = \frac{1}{4F}(\mu_{O_2(a)} - \mu_{O_2,R}), \qquad [7]$$

where $\mu_{O_2,R}$ is the chemical potential of oxygen at the reference (R) electrode; $\mu_{O_2,R}$ is always equal to the chemical potential $\mu_{O_2,R(g)}$ of oxygen in the reference gas phase, i.e., in air. The chemical potential $\mu_{O_2(a)}$, however, of oxygen adsorbed on the catalyst surface does not, in general, equal the gas phase oxygen chemical potential in the cell $\mu_{O_2(g)}$ during the PPR measurements. When $\mu_{O_2(a)}$ and $\mu_{O_2(g)}$ are equal, e.g., at the end of the adsorption process, when equilibrium for oxygen adsorption is established, then Eq. [7] reduces (Ref. (1)) to the usual Nernst equation

$$E = V^0_{WR} = \frac{RT}{4F} \ln (P_{O_2}/P_{O_2,R}), \qquad [8]$$

where P_{O_2} and $P_{O_2,R}$ are the oxygen partial pressures in the cell and the reference air compartment, respectively.

During oxygen desorption, however, $\mu_{O_2(g)}$ is significantly lower than $\mu_{O_2(a)}$. In fact, it is the difference

$\mu_{O_2(a)} - \mu_{O_2(g)}$ which is the driving force for oxygen desorption. By taking into account that

$$\mu_{O_2,R} = \mu^\circ_{O_2} + 4FV_R, \quad [9]$$

where V_R is the reference electrode potential (p_{O_2} = 21 kPa) with respect to the standard oxygen electrode potential (p_{O_2} = 101.3 kPa) and $\mu^\circ_{O_2}$ is the standard (p_{O_2} = 101.3 kPa) chemical potential of gaseous oxygen at the operating temperature T, it follows from Eq. [7] that

$$E_p = -V_R + \frac{1}{4F}(\mu_{O_2(a)} - \mu^\circ_{O_2}), \quad [10]$$

where the reference electrode V_R is easily computable via

$$V_R = \frac{RT}{4F} \ln (21 \text{ kPa}/101.3 \text{ kPa}) = -0.39\, RT/F. \quad [11]$$

When oxygen is adsorbed associatively, i.e.,

$$O_2(g) \rightarrow O_2(a), \quad [12]$$

then it follows from Eq. [10] that the standard Gibbs free energy change ΔG° of the adsorption process (12) is

$$\Delta G^\circ = \mu_{O_2(a)} - \mu^\circ_{O_2} = 4F(E_p + V_R) \quad [13]$$

or, equivalently,

$$\Delta G^\circ = 4FE_{p,rev}, \quad [14]$$

where

$$E_{p,rev} = E'_p + V_R \quad [15]$$

and E'_p is the extrapolated E_p value for $\upsilon = 0$. It should be noted that the standard state of adsorbed oxygen in Eqs. [13] and [14] is that corresponding to the operating temperature T and to the potential $E_{p,rev}$.

When oxygen is adsorbed dissociatively, i.e.,

$$O_2(g) \rightarrow 2O(a), \quad [16]$$

then the chemical potential $\mu_{O_2(a)}$ can be expressed as $\mu_{O_2(a)} = 2\mu_{O(a)}$, where μ_O is the chemical potential of adsorbed atomic oxygen and $2\mu_O$ expresses the chemical potential of gaseous oxygen that would be in equilibrium with adsorbed oxygen if such an equilibrium were established (1). Therefore, Eq. [10] is written:

$$E_p = -V_R + \frac{1}{4F}(2\mu_{O(a)} - \mu^\circ_{O_2}). \quad [17]$$

Consequently the ΔG° of the adsorption process (16) can be written as

$$\Delta G^\circ = 2\mu_O - \mu^\circ_{O_2} = 4F(E_p + V_R), \quad [18]$$

and thus Eq. [14] is obtained again. In the above expression the atomic adsorbed oxygen standard state is again that corresponding to $E_{p,rev}$ and T. Consequently Eq. [14] holds regardless of the associative, dissociative, or subsurface nature of oxygen adsorption.

As an example, at 380°C (Figs. 3 and 4) $E_{p,rev}$ is −115 mV for peak A and −240 mV for peak B. Consequently ΔG° is computed to equal −10.6 and −22 kcal/mol O_2, respectively.

Since from thermodynamics

$$\Delta G^\circ = \Delta H^\circ - T\Delta S^\circ \quad [19]$$

one can rewrite Eq. [14] as

$$E_{p,rev} = \frac{\Delta H^\circ}{4F} - T\,\frac{\Delta S^\circ}{4F}. \quad [20]$$

It therefore follows that by studying the temperature dependence of $E_{p,rev}$ one can extract both the standard enthalpy change and standard entropy change of the adsorption process (16). The former equals the negative of the heat of adsorption.

Figure 10 shows the effect of temperature and t_{He} on the PPR spectra of oxygen adsorbed on Ag, obtained at constant υ. At lower temperatures, the peak separation is not good because the electroreduction kinetics are slow and the peaks are not reversible. Thus lower υ value had to be used to ensure reversibility at the low temperature range to extract the $E_{p,rev}$ vs T dependence shown in Fig. 11. As shown in Fig. 11, $E_{p,rev}$ increases with T in good qualitative agreement with Eq. [20], since ΔS° is expected to be negative for a chemisorptive process. By combining Fig. 11 and Eq. [20] one obtains

$$\Delta H^\circ_A = -18(\pm 9)\text{kcal/mol}, \Delta S^\circ_A = -12(\pm 7)\text{cal/mol}\cdot\text{K},$$

$$\Delta H^\circ_B = -50(\pm 20)\text{kcal/mol}, \quad \text{and}$$

$$\Delta S^\circ_B = -38(\pm 17)\text{cal/mol}\cdot\text{K},$$

where the error limits correspond to a 95% statistical confidence level.

The ΔH°_A value is in very good agreement with the measured activation energy for atomic oxygen desorption (20 kcal/mol). The ΔS°_A value is small but reasonable if one takes into account the expected high surface mobility of adsorbed atomic oxygen. The $-\Delta H^\circ_B$ and $-\Delta S^\circ_B$ values

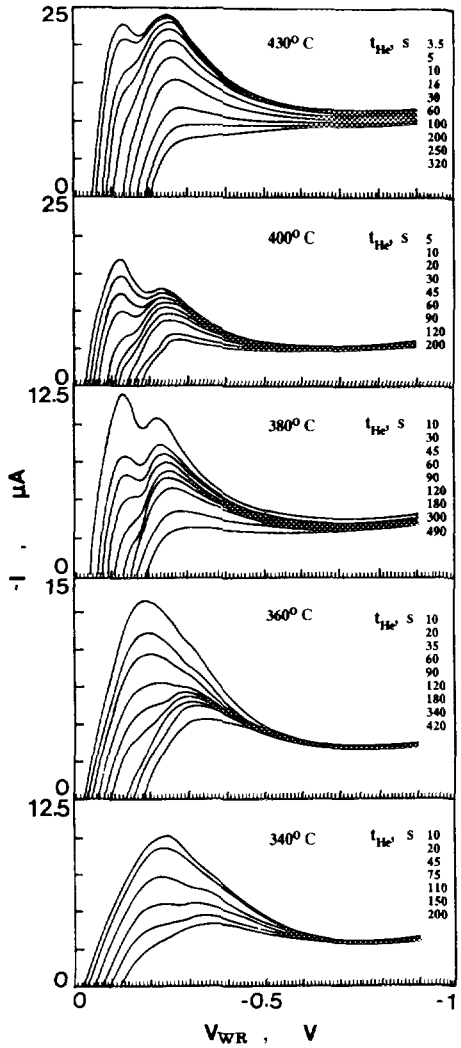

FIG. 10. Temperature effect on the PPR spectra of oxygen adsorbed on Ag; t_H = 60 s, V_{WR} = 0.2 V, F_{He} = 100 cm³ STP/min, ν = 20 mV/s for T = 430°C, and ν = 10 mV/s for other temperatures.

for subsurface oxygen are both high but reasonable. In general the $E_{p,rev}$ variation with T is rather small (~30 mV for each 100 K) and consequently the determination of ΔH^0 and ΔS^0 is subject to significant experimental error in the present exploratory study. Nevertheless, Eqs. [14] and [20] in conjunction with PPR offer, in principle, a unique opportunity to study the thermodynamics of adsorption on metal surfaces.

Pt Catalyst Films

The chemisorption of oxygen on Pt surfaces has been the subject of numerous papers and reviews (46–51). There is general agreement that above 300 K oxygen adsorption is dissociative. The adsorption/desorption kinetics have been studied by TPD (46–51), molecular beam scattering (50), Auger spectroscopy (51), and work function measurements (47). On Pt (111) the atomic oxygen peak desorption temperature is near 450°C (usually denoted as β-state), while molecularly adsorbed oxygen which desorbs below 300 K is usually termed the α-state (48). The desorption kinetic constant k_d from the Pt(111) surface, which is expected and has been shown by STM (1) to be the dominant surface plane of the polycrystalline films used here, has been expressed by Campbell *et al.* (50) as

$$k_d = \nu_2 \exp[-(E_{d,O} + \omega\theta_O)/RT], \qquad [21]$$

with $\nu_2 = 2.4 \times 10^{-2}$ (cm$_2$/s · atom), $E_{d,O}$ = 50.9 kcal/mol, and ω = −10.0 kcal/mol, and by Yates and co-workers (48) by the same expression with $E_{d,O}$ = 48.0 kcal/mol, ω = −5.3 kcal/mol, and $\nu_2 = 1.5 \times 10^{-3}$ (cm²/s · atom). As shown below, these kinetic constants are in excellent agreement with the present results.

On stepped surfaces, e.g., Pt(112), Yates and co-workers (48) found that the β-state splits into two states β_1 and β_2 of which the more weakly bound state β_1 exhibits attractive lateral interactions and the β_2 state exhibits repulsive lateral interactions (48).

Figure 12 shows typical PPR spectra obtained with a polycrystalline Pt film after dosing with oxygen through the solid electrolyte (V_{WR} = 0.2 V for 30 s). When low oxygen potentials are used, only one oxygen peak is obtained as shown in Fig. 12. This peak clearly corresponds to atomic oxygen, i.e. to peak "β" in TPD spectra of oxygen on Pt (48). The E_p value is between −50 and −150 mV and, as also shown in Fig. 12 and discussed below, increases with increasing temperature. This is consistent with the negative ΔS^0 of oxygen adsorption (Eq. [15]). Figure 12 also depicts the effect of desorption time (t_{He}) on the PPR spectrum and consequently also demonstrates that oxygen coverage has an important effect on E_p. At

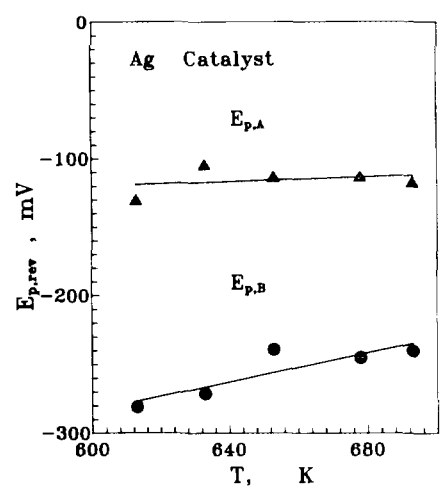

FIG. 11. Temperature effect on the reversible peak potentials, $E_{p,rev}$, of oxygen peaks A (atomic oxygen) and B (subsurface oxygen).

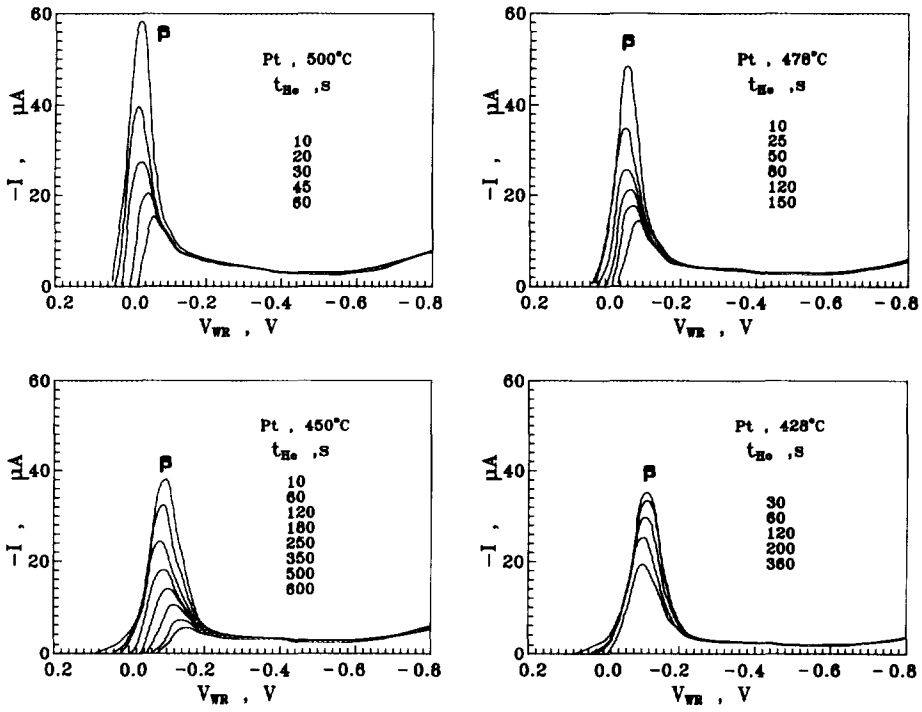

FIG. 12. Effect of desorption time t_{He} and temperature on the PPR spectrum of oxygen adsorbed on Pt; t_H = 30 s, V_{WR} = 0.2 V, v = 10 mV/s, F_{He} = 100 cm³ STP/min.

higher temperatures (478° and 500°C) E_p shifts to more positive potentials with increasing oxygen coverage. This could imply either strong repulsive interactions between the adsorbed oxygen atoms or significant heterogeneity of the adsorption sites on the polycrystalline Pt film, with the lower energy sites occupied first, or both. However, as also shown in Fig. 12 at lower temperatures (T = 428°C) the situation changes and E_p shifts to more negative potentials with increasing oxygen coverage. This shows that adsorption site heterogeneity must play a limited role. This observation is clearly indicative of attractive interactions between the adsorbed oxygen atoms. This is in excellent agreement with the work of Yates and co-workers (48), who have found that on Pt(112) there exist two atomic adsorption states (β_1, β_2) with desorption maxima at 417 and 487°C, of which the more weakly bound state β_1 exhibits attractive interactions and the more strongly bound state β_2 exhibits repulsive interactions. This behaviour is nicely manifested in Fig. 12 (T = 450°C) where, upon decreasing oxygen coverage, E_p first increases (attractive interactions corresponding to desorption of the more weakly bound oxygen, i.e., state β_1 of Yates and co-workers) and then decreases (repulsive interactions corresponding to desorption of the more strongly bound oxygen, i.e., state β_2 of Yates and co-workers).

These trends are shown clearly in Figs. 13 and 14. Thus Fig. 13 shows the effect of the amount of oxygen adsorbed at the tpb ($N_{O,tpb}$) computed by integration of the PPR peaks (Eq. [6]) and of the relative oxygen coverage θ_O on the peak potential E_p. The relative oxygen coverage θ_O scale has been constructed by assigning the value of unity to the maximum measured amount of oxygen adsorbed at the tpb, i.e., 2.6 × 10^{-9} g-atom O.

As shown in Fig. 13 repulsive interactions (increasing E_p) dominate at low coverages and attractive interactions (decreasing E_p) appear at high coverages.

By cross plotting the data of Fig. 13 one obtains Fig. 14, which depicts the effect of temperature on E_p at constant

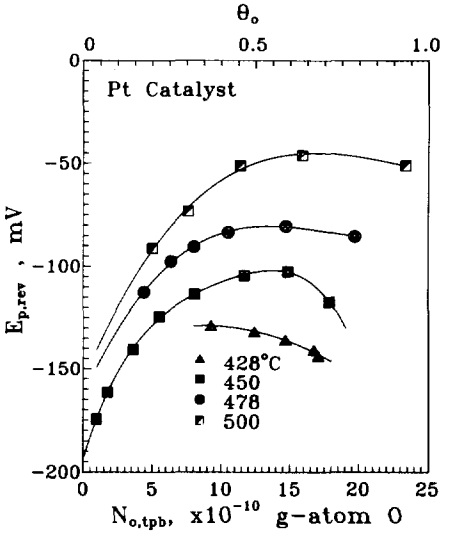

FIG. 13. Effect of the amount of adsorbed oxygen and of oxygen coverage on the peak potential of atomic oxygen on Pt.

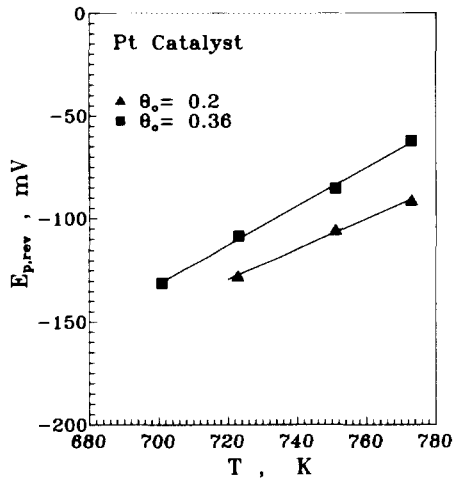

FIG. 14. Temperature effect on the peak potential of atomic oxygen on Pt at constant oxygen coverage.

values of the oxygen coverage. The observed linear dependence conforms nicely to Eq. [20]. However, as discussed below, the extracted ΔH° and ΔS° values can be taken only as first approximations.

As shown in Fig. 15 prolonged ($t_H > 100$ s) application of a more positive potential ($V_{WR} = 0.3$ V) leads to the formation of a second oxygen peak (labeled δ in Fig. 15). This second peak has also been obtained during cyclic voltammetric investigation of Pt electrodes deposited on YSZ (32).

It has been also recently shown by XPS (28) that prolonged application of positive V_{WR} values results in the spillover of significant amounts of oxidic oxygen from the YSZ lattice on the Pt surface. The coverage of this anionic and relatively unreactive (28) oxygen species with O1*s* binding energy at 528.8 eV (vs 530 eV for normally chemisorbed atomic oxygen (28)) can be comparable to that of normally chemisorbed oxygen as the two species coexist on the Pt surface (28). This anionic oxygen species has been shown to act as a promoter by weakening the Pt-atomic oxygen bond (1, 11, 28) and to cause NEMCA when using YSZ as the solid electrolyte (28). Consequently the second oxygen peak labeled δ in Fig. 15 must be attributed to spillover oxidic oxygen (28). The fact that the E_p of the δ-state is more negative than the E_p of the β-state (normally chemisorbed atomic oxygen) is consistent with its significantly lower reactivity (1, 28) which allows it to act as a promoter in NEMCA studies (1, 28). The possible relationship of this anionic oxygen species with the formation of subsurface oxygen or surface PtO_2 (52–56) is not yet clear. The present exploratory PPR study has focused on normally chemisorbed atomic oxygen, i.e., peak β.

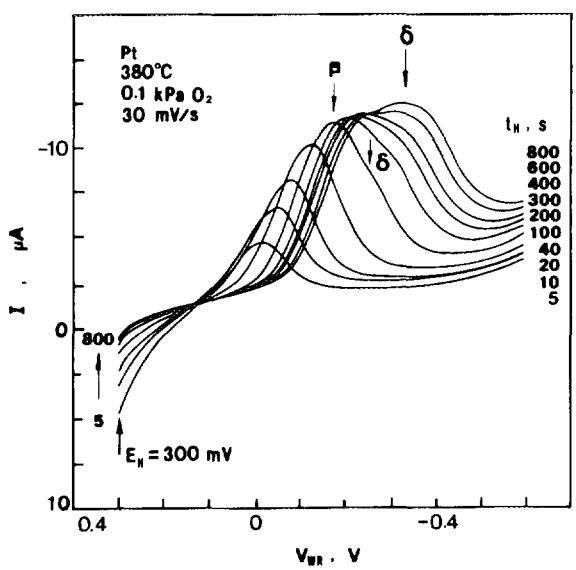

FIG. 15. Effect of holding time t_H at a potential $V_{WR} = 0.3$ V on the PPR spectrum of oxygen adsorbed on Pt at $P_{O_2} = 0.1$ kPa; $v = 30$ mV/s, $F_{He} = 100$ cm³ STP/min.

Desorption kinetics. Figure 16 shows the kinetics of atomic oxygen desorption; i.e., it depicts the time evolution of $N_{O,tpb}$ computed by integration of the PPR peaks (Eq. [6]). The maximum amount of oxygen adsorbed at the tpb is 2.6×10^{-9} g-atom O. Similarly to the case of atomic oxygen desorption from Ag, the kinetics can be adequately described as a first-order desorption process (Fig. 16). Similar behaviour has been observed for the desorption of atomic oxygen from polycrystalline Pt films when using the isothermal desorption-surface titration technique (1, 5, 8). Most previous workers have extracted a modified second-order dependence from their TPD spectra with a coverage-modified desorption activation energy (48, 50), i.e., Eq. [21], but in reality the situation is more complex, as shown by the isothermal desorption spectra of Yates and co-workers (48) and by the "autocatalytic" nature of the desorption of the β_1-state from Pt(112) (48). It is likely that the difference in the observed apparent

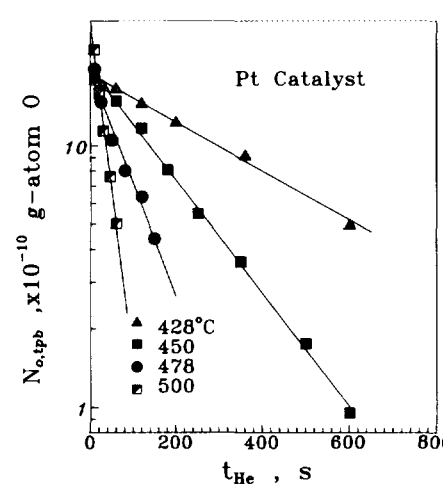

FIG. 16. Temperature effect on the kinetics of atomic oxygen desorption from Pt.

desorption kinetics may be due to the higher pressures of the present investigation although, as subsequently shown, there is excellent qualitative agreement regarding the normalized values (molecules/(cm^{2}s)) of atomic oxygen desorption from the present study and from the studies of Campbell *et al.* (50) and of Yates and co-workers (48).

Figure 17 shows the temperature dependence of the first-order desorption rate constant $k_d(s^{-1})$ obtained from the slopes of Fig. 16. The extracted desorption activation energy (40 kcal/mol) is in reasonable agreement with literature values for high oxygen coverages (46–51).

Figure 18 compares the normalized desorption rate R_d values (molecules/cm^{2}s)) of atomic oxygen from the present work and from the works of Campbell *et al.* (50) and of Yates and co-workers (48). To this end we have used the Pt(111) surface density ($d = 1.5 \times 10^{15}$ atoms/cm^2) and a maximum absolute oxygen coverage of 0.25 (48, 50) to express our data on the basis of the observed first order desorption kinetics (Fig. 17), i.e.,

$$R_d = (0.25d)k_d\theta_O. \qquad [23]$$

The computed values are compared with those directly computed from Refs. (48) and (50) via Eq. [21]. The observed excellent qualitative agreement corroborates the reliability of the PPR technique for studying desorption kinetics.

Thermodynamic considerations. The measured E_p values for the β-state of oxygen are of the order of -100 mV (Figs. 12–15) and allow, in principle, the computation of $\Delta G°$ for the adsorption process (16) via Eqs. [14] and [15]. Thus at 450°C and a relative oxygen coverage of 0.5 it is $E_{p,rev} \approx -110$ mV, and consequently $\Delta G°$ is estimated to be -10 kcal/mol O_2. As shown in Fig. 13 for low θ_O values E_p increases with θ_O and the increase is almost

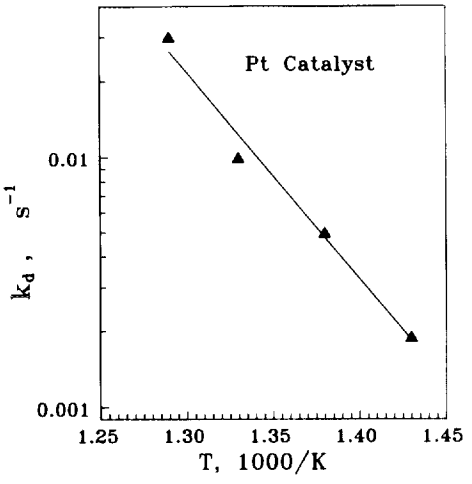

FIG. 17. Arrhenius plot of the desorption rate constant k_d of atomic oxygen.

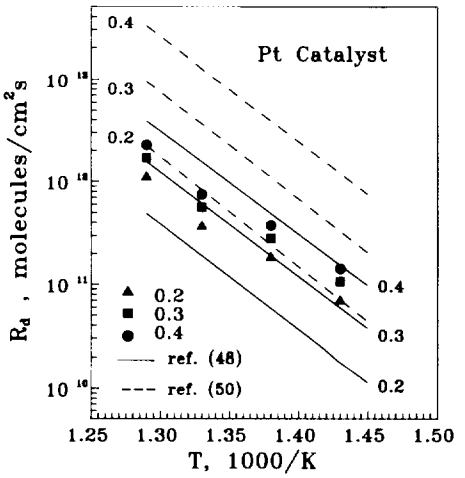

FIG. 18. Effect of temperature on the normalized atomic oxygen desorption rate measured at $\theta_0 = 0.2$, 0.3, and 0.4 and comparison with literature values for Pt(111) obtained via TPD for the same relative oxygen coverages (Eq. [16]).

linear, consistent with the assumptions of the Temkin isotherm (31), i.e., consistent with a linear decrease in the heat of adsorption with coverage due to lateral repulsive interactions. For higher θ_O values E_p starts to decrease with θ_O, which indicates attractive lateral interactions, consistent with the observations of Yates and co-workers for the more weakly bound state β_1 (48).

The observed linear increase in E_p with T at fixed θ_O (Fig. 14) is consistent with Eq. [20]. It gives $-\Delta H°$ values of 60(±25) kcal/mol, where again the error limits correspond to a 95% statistical confidence level. The average value of 60 kcal/mol is somehow larger than expected (46–51) for the relatively high oxygen coverages of this investigation and also larger than the measured activation energy of desorption (40 kcal/mol). The computed $-\Delta S°$ values are -67 (±35) cal/mol · K. The average is significantly larger than the expected -40 to -45 cal/mol · K (53). However, it is quite reassuring for the PPR technique that all the literature $-\Delta H°$ and $-\Delta S°$ values (46–53) are within the undoubtedly broad error limits of the present exploratory study. In general the extraction of $\Delta H°$ and $\Delta S°$ via the temperature dependence of E_p is expected to be less accurate than the extraction of $\Delta G°$. There are, however, two additional factors which must have contributed to the high computed average values of $|\Delta H°|$ and $|\Delta S°|$ in the present study. First, there must have been some irreverisiblity of the PPR oxygen peak. Since Pt is not as good an electrocatalyst as Ag for the charge-transfer reaction (2) and (3) (Ref. (1)), i.e., since it has in general a lower I_0 value than Ag (1), it follows that it is in general more difficult to obtain a truly reversible oxygen reduction peak (36). Second, it is well established (1, 19–21) that application of negative potentials, i.e., decreasing catalyst work function in the type of solid electrolyte supported catalysts studied here, causes in general

a strengthening in the Pt–O bond (1, 11). This is qualitatively consistent with the measured higher $|\Delta H^\circ|$ values. Thus a negative overpotential of 0.15 V, causing (1, 11) a work function decrease of 0.15 eV, is expected to cause an increase up to 0.15 eV/atom O, i.e., up to 7 kcal/mol O_2 in the heat of adsorption of oxygen relative to its open-circuit value (1, 19). This change in binding strength with changing catalyst potential and work function is intimately related to the origin of NEMCA (1, 11, 19) and is consequently a small disadvantage of the PPR technique. Nevertheless, at least in the present case of oxygen chemisorption on Ag and Pt, and peak potentials E_p appear at relatively small overpotentials (-0.1 to -0.25 V) and consequently the increase in the binding strength of electron-acceptor adsorbates, such as oxygen, is rather moderate.

CONCLUSIONS

Preliminary experiments have shown that PPR is a useful new technique for detecting different oxygen species on conductive catalysts. The PPR technique can give useful information about the thermodynamics of adsorption (ΔG° and via temperature variation ΔH° and ΔS°) and can be used for the investigation of adsorption and desorption kinetics. The main disadvantage of the technique is that it is limited to conductive catalysts supported on solid electrolytes. Also the applied potential may have a moderate effect on the measured kinetic and thermodynamic quantities. The main advantages are isothermality and *in situ* applicability without any high vacuum requirements.

REFERENCES

1. Vayenas, C. G., Bebelis, S., Yentekakis, I.V., and Lintz, H-G., *Catal. Today* **11**(3), 303 (1992).
2. Wagner, C., *Adv. Catal.* **21,** 323 (1970).
3. Vayenas, C. G., and Saltsburg, H. M., *J. Catal.* **57,** 296 (1979).
4. Stoukides, M., and Vayenas, G. C., *J. Catal.* **74,** 266 (1982).
5. Vayenas, G. C., Lee, B., and Michaels, J. N. *J. Catal.* **66,** 36 (1980).
6. Stoukides, M., and Vayenas, C. G., *J. Catal.* **82,** 45 (1983).
7. Hafele, E., and Lintz, H-G., *Ber. Bunsenges. Phys. Chem.* **90,** 288 (1986).
8. Yentekakis, I. V., Neophytides, S., and Vayenas, C. G., *J. Catal.* **111,** 152 (1988).
9. Vayenas, C. G., Georgakis, C., Michaels, J. N., and Tormo, J., *J. Catal.* **67,** 348 (1981).
10. Ladas, S., Bebelis, S. and Vayenas, C.G., *Surf. Sci.* **251/252,** 1062 (1991).
11. Vayenas, C. G., Bebelis, S., and Ladas, S., *Nature (London)* **343,** 625 (1990).
12. Singhal, S. C., *in* "Proceedings, 2nd International Symposium on Solid Oxide Fuel Cells, Athens, Greece 1990," pp. 25. EEC, Luxembourg, 1991.
13. Grosz, F., *in* "Proceedings, 2nd International Symposium on Solid Oxide Fuel Cells, Athens, Greece 1990," p. 7. EEC, Luxembourg, 1991.
14. Vayenas, C. G., and Farr, R. D., *Science* **208,** 593 (1980).
15. Kiratzis, N., and Stoukides, M., *J. Electrochem. Soc.* **134,** 1925 (1987).
16. Yentekakis, I. V., and Vayenas, C. G., *J. Electrochem. Soc.* **136,** 996 (1989).
17. Yentekakis, I. V., and Vayenas, C. G., *J. Catal.* **111,** 170 (1988).
18. Vayenas, C. G., Bebelis, S., and Neophytides, S., *J. Phys. Chem.* **92,** 5083 (1988).
19. Bebelis, S., and Vayenas, C. G., *J. Catal.* **118,** 125 (1989).
20. Neophytides, S., and Vayenas, C. G., *J. Catal.* **118,** 147 (1989).
21. Bebelis, S., and Vayenas, C. G., *J. Catal.* **138,** 570 (1992).
22. Bebelis, S., and Vayenas, C. G., *J. Catal.* **138,** 588 (1992).
23. Marina, O. A., and Sobyanin, V. A., *Catal. Lett.* **13,** 61 (1992).
24. Eng, S., and Stoukides, M., *J. Catal.* **130,** 306 (1991).
25. Stoukides, M., and Vayenas, C. G., *J. Catal.* **70,** 137 (1981).
26. Cavalca, C., Larsen, G., Vayenas, C. G., and Haller, G. L., *J. Phys. Chem.* **97,** 6115 (1993).
27. Yentekakis, I. V., Moggridge, G., Vayenas, C. G. and Lambert, R. M., *J. Catal.* **146,** 292 (1994).
28. Ladas, S., Kennou, S., Bebelis, S., and Vayenas, C. G., *J. Phys. Chem.* **97,** 8845 (1993).
29. Pliangos, C., Yentekakis, I. V., Verykios, X. E., and Vayenas, C. G., in preparation (1994).
30. Pritchard, J., *Nature (London)* **343,** 592 (1990).
31. Vayenas, C. G., Ioannides, A., and Bebelis, S., *J. Catal.* **129,** 67 (1991).
32. Yi, Jiang, Kaloyannis, A., and Vayenas, C. G., *Electrochim. Acta* **38,** 2533 (1993).
33. Yang, C. Y., and Isaacs, H. S., *J. Electroanal. Chem. Interfacial Electrochem.* **123,** 411 (1981).
34. Gozzi, D., Tomellini, M., Petrucci, L., and Cignini, P. L. *J. Electrochem. Soc.* **134,** 728 (1989).
35. P. A. Van Manen, Weewer, R., and Dewit, J. H. W., *J. Electrochem. Soc.* **139,** 1130 (1992).
36. Bard, A. J., and Faulkner, L. R., "Electrochemical Methods: Fundamentals and Applications." Wiley, New York, 1980.
37. Laviron, E., *J. Electroanal. Chem. Interfacial Electrochem.* **101,** 19 (1979).
38. Angerstein-Kozlowska, H., Klinger, J., and Conway, B. E., *J. Electroanal. Interfacial Electrochem.* **75,** 45 (1977).
39. Grant, R. B., and Lambert, R. M., *Surf. Sci.* **146,** 256 (1984).
40. R. A. Van Santen, and Kuipers, H. P. C. E., *Adv. Catal.* **35,** 365 (1987).
41. Campbell, C. T., and Paffett, M. T., *Surf. Sci.* **143,** 517 (1984).
42. Kitson, M., and Lambert, R. M., *Surf. Sci.* **109,** 60 (1981).
43. Kitson, M., and Lambert, R. M., *Surf. Sci.* **110,** 205 (1981).
44. Tan, S. A., Grant, R. B., and Lambert, R. M., *J. Catal.* **106,** 54 (1987).
45. Xinhe, B., and Jingfa, D., *Surf. Sci.* **163,** 444 (1985).
46. Gland, J. L., *Surf. Sci.* **93,** 487 (1980).
47. Derry, G. N., and Ross, P. N., *J. Chem. Phys.* **82,** 2772 (1985).
48. Winkler, A., Guo, X., Siddiqui, H. R., Hagans, P. L., and Yates, J. T., Jr., *Surf. Sci.* **201,** 419 (1988).
49. Akhter, S., Greenlief, C. M., Chen, H.-W., and White, J. M., *Appl. Surf. Sci.* **25,** 154 (1986).
50. Campbell, C. T., Ertl, G., Kuipers, H., and Segner, J., *Surf. Sci.* **107,** 220 (1981).
51. Gland, J. L., Sexton, B. A., and Fisher, J. B., *Surf. Sci.* **95,** 587 (1980).
52. Berry, J., *Surf. Sci.* **76,** 415 (1978).
53. Vayenas, C. G., Lee, B., and Michaels, J. N., *Surf. Sci.* **120,** L405 (1982).
54. Peuckert, M., and Ibach, H., *Surf. Sci.* **136,** 319 (1984).
55. Peuckert, M., and Bonzel, H. P., *Surf. Sci.* **145,** 239 (1984).
56. Peuckert, M., *J. Phys. Chem.* **89,** 2481 (1985).